Journal of Materials Chemistry C

COMMUNICATION

View Article Online
View Journal | View Issue

Cite this: J. Mater. Chem. C, 2019, 7, 6236

Received 2nd April 2019,
Accepted 8th May 2019

DOI: 10.1039/c9tc01765h

rsc.li/materials-c

Low-dimensional non-toxic $A_3Bi_2X_9$ compounds synthesized by a dry mechanochemical route with tunable visible photoluminescence at room temperature†

Yousra El Ajjouri,[a] Vladimir S. Chirvony,[ab] Natalia Vassilyeva,[a] Michele Sessolo,[a] Francisco Palazon *[a] and Henk J. Bolink[a]

We have synthesized fifteen inorganic and hybrid organic–inorganic non-toxic $A_3Bi_2X_9$ compounds (A = K^+, Rb^+, Cs^+, $CH_3NH_3^+$ and $HC(NH_2)_2^+$; X = I^-, Br^-, Cl^-) through dry mechanochemistry. We demonstrate that this synthetic method is very well suited to prepare compounds from poorly soluble precursors, allowing thus the preparation of so far unreported compounds. X-ray diffraction analysis demonstrates the high crystallinity of the so-formed ternary bismuth halides. Furthermore, we show that, through substitution of the A-cation and X-anion, the bandgap of these compounds can be tuned to absorb throughout the whole visible spectrum. As-prepared powders of $Cs_3Bi_2Br_9$ and $Cs_3Bi_2I_9$ without any passivating agents show room-temperature photoluminescence covering the visible spectrum from 450 nm to 800 nm, making them especially promising for white-light emission.

Over the past decade, lead-halide perovskites (LHPs) have been intensively investigated due to their excellent optoelectronic properties. These are the result, among other reasons, of the intrinsic point defect tolerance of LHPs, which has been suggested to be crucial in achieving long charge carrier diffusion lengths, enabling high efficiencies in perovskite devices.[1] However, the future commercialization of state-of-the-art perovskite optoelectronic devices is hampered by the use of toxic lead and the unclear environmental stability of LHPs. Therefore, lead-free perovskite alternatives are being sought. The defect-tolerant character of LHPs has been linked to the presence of the ns^2 electron lone pair in Pb^{2+}, a characteristic that is shared with Bi^{3+} which has a $6s^2$ electron configuration.[2–7] Hence, Bi(III)-halide compounds are envisioned as interesting alternatives, with potentially the same defect tolerance as LHPs. Moreover, bismuth is a very abundant element, as well as non-toxic and stable in ambient conditions.[3] The replacement of Pb^{2+} with Bi^{3+} affects the stoichiometry of the ternary metal halides. The general formula for LHPs can be written as $APbX_3$ where A is a monovalent cation and X a monovalent halide anion. The bismuth-counterparts, however, have a "3-2-9" stoichiometry corresponding to the general formula $A_3Bi_2X_9$. This is sometimes seen as a "defect" or "vacancy-ordered" perovskite. As explained by McCall *et al.* "defect perovskites are derivative structures that possess the same corner-sharing MX_6 octahedra as the AMX_3 aristotype but form different structures due to cation deficiencies in order to satisfy charge balance restrictions... trivalent cations form $A_3M_2\square X_9$ structures [□ represents a vacancy] with 2/3 occupancy of the M sites of the $A_3M_3X_9$ perovskite formula".[8] In the case of $A_3Bi_2X_9$ compounds, different crystal structures are obtained by varying the chemical composition. As an example, while $Cs_3Bi_2I_9$ crystallizes in a zero-dimensional structure with fully decoupled dimers of BiI_6 octahedra, $Rb_3Bi_2I_9$ crystallizes in a 2D structure with layers of corner-sharing BiI_6 octahedra (see Scheme 1).[9] This reduced dimensionality is the reason why these compounds

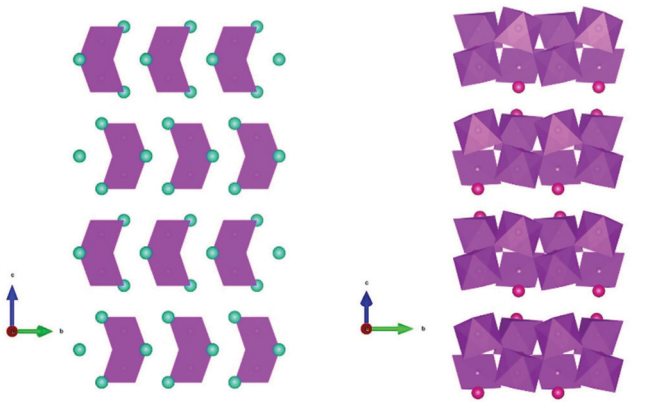

Scheme 1 $Cs_3Bi_2I_9$ (left) and $Rb_3Bi_2I_9$ (right) crystal structures, viewed from the a-axis. $Cs_3Bi_2I_9$ presents a zero-dimensional structure with dimers of BiI_6 octahedra (pink) fully decoupled while $Rb_3Bi_2I_9$ presents a 2D structure with layers of corner-sharing BiI_6 octahedra. Green and red balls represent Cs^+ and Rb^+ cations.

[a] Instituto de Ciencia Molecular, Universidad de Valencia, C/ Catedrático J. Beltrán 2, 46980 Paterna, Spain. E-mail: francisco.palazon@uv.es
[b] UMDO (Unidad de Materiales y Dispositivos Optoelectrónicos), Instituto de Ciencia de los Materiales, Universidad de Valencia, Valencia 46071, Spain

† Electronic supplementary information (ESI) available: Experimental details and XRD. See DOI: 10.1039/c9tc01765h

are also referred to as low-dimensional perovskites, although the term perovskite is questionable here.

One of the main bottlenecks in developing bismuth-halide-based compounds resides in the poor solubility of bismuth salts in common solvents.[10,11] In this study, fifteen different $A_3Bi_2X_9$ compounds (A = K^+, Rb^+, Cs^+, $CH_3NH_3^+$ –MA–, and $HC(NH_2)_2^+$ –FA–; X = I^-, Br^-, Cl^-) were synthesized by a dry mechanochemical approach *via* ball-milling of stoichiometric precursors. This technique allows the formation of multinary metal halide compounds in a simple and time-efficient manner.[12–15] To the best of our knowledge, there is only one previous report on dry mechanochemical synthesis of ternary bismuth-iodide compounds.[16] We are unaware of reports about the synthesis (through any method) of several of the chloride and bromide analogues such as $FA_3Bi_2Br_9$, $FA_3Bi_2Cl_9$ or $Rb_3Bi_2Cl_9$. Hereby, we investigate the structural and optical characteristics of the fifteen compounds described above. X-ray diffraction (XRD) analyses show the excellent crystal quality of mechanochemically-synthesized powders. These have a tunable bandgap from the near-UV to the red part of the visible spectrum as shown by optical absorption. Furthermore, bulk $Cs_3Bi_2I_9$ and $Cs_3Bi_2Br_9$ show a broad visible photoluminescence at room temperature, even without the addition of passivating agents. This paves the way to the use of these materials for lighting applications.

Powders obtained by ball-milling stoichiometric amounts of inorganic AX and BiX_3 were analyzed by XRD (see Fig. 1). In the five cases ($Cs_3Bi_2I_9$, $Cs_3Bi_2Br_9$, $Cs_3Bi_2Cl_9$, $Rb_3Bi_2I_9$, and $Rb_3Bi_2Br_9$) where we could compare the diffractograms with bulk reference patterns published in the Inorganic Crystal Structure Database (ICSD), excellent matches are obtained. This points towards the high phase-purity obtained with this simple and dry method. No published reference pattern was found for $Rb_3Bi_2Cl_9$. However, when compared to $Rb_3Bi_2I_9$ and $Rb_3Bi_2Br_9$, a clear gradual shift towards higher angles (smaller interatomic distances) is visible when the halide ionic radius is reduced from I^- to Cl^-. This suggests a shrinkage of the unit cell. In order to assess this more accurately, whole-pattern Le Bail fits were conducted on all three $Rb_3Bi_2X_9$ compounds (see Fig. S2, ESI†). The refined cell parameters and unit cell volume are summarized in Table 1. This is strong evidence for the formation of $Rb_3Bi_2Cl_9$, which to the best of our knowledge has not been experimentally synthesized before. The potassium-based series

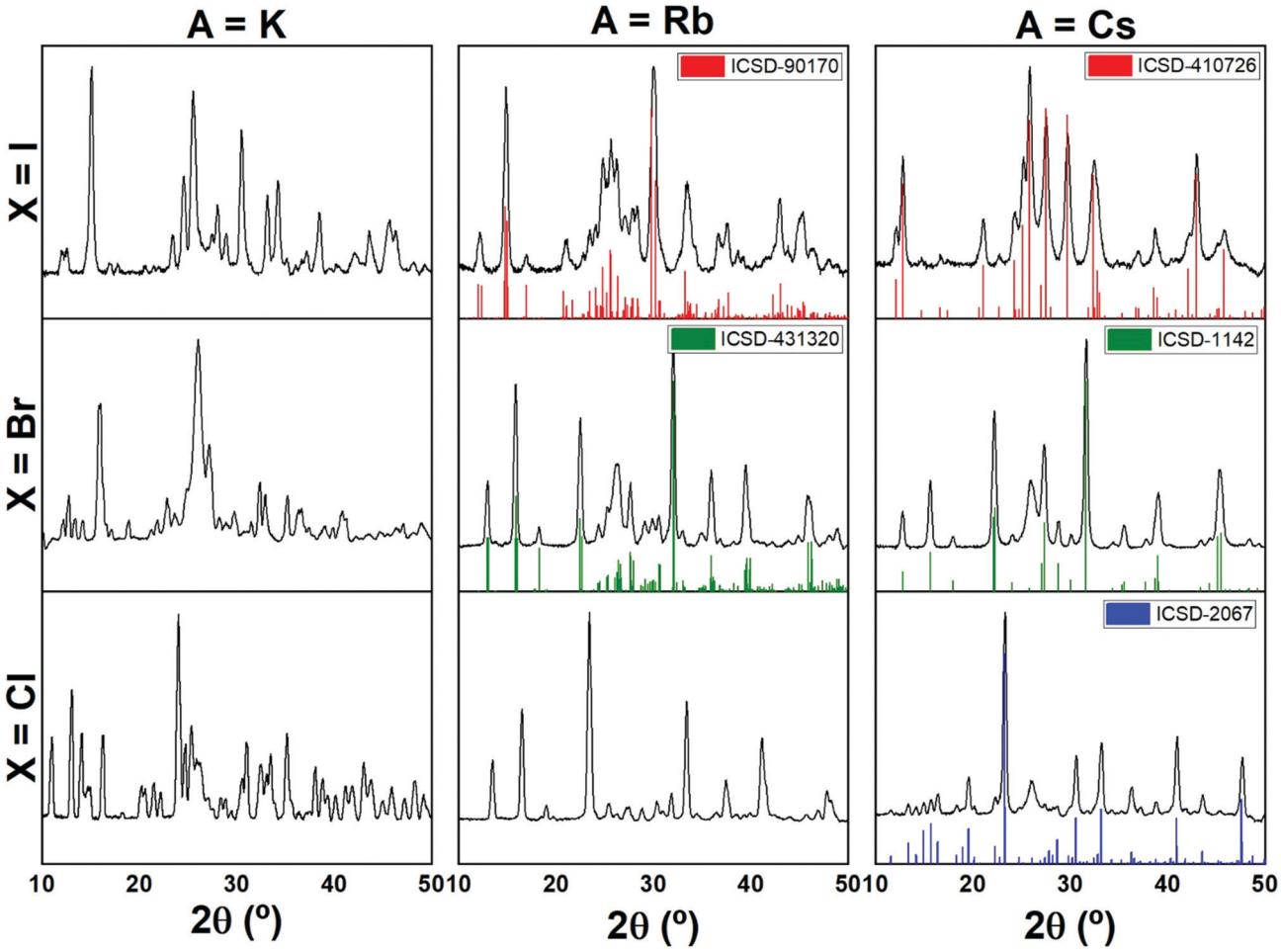

Fig. 1 XRD characterization of mechanochemically-synthesized inorganic $A_3Bi_2X_9$ (A = K, Rb, Cs; X = I, Br, Cl; black lines) and reference bulk patterns when available from the Inorganic Crystal Structure Database (ICSD; color columns). A broad feature around $2\Theta = 26^\circ$ is sometimes visible, due to the parasitic diffraction of the underlying adhesive tape used to fix the powder samples on the holder (see Fig. S1, ESI†).

Table 1 Refined cell parameters for $Rb_3Bi_2X_9$ compounds

	Reference	This work
$Rb_3Bi_2I_9$ ($P1c1$)	a = 14.690 Å b = 8.195 Å c = 25.645 Å V = 2516.82 Å^3	a = 14.6874(8) Å b = 8.1982(6) Å c = 25.646(1) Å V = 2517.5(3) Å^3
$Rb_3Bi_2Br_9$ ($P12_1/a1$)	a = 13.5601(1) Å b = 7.9124(5) Å c = 19.3510(8) Å V = 2076.13 Å^3	a = 13.570(1) Å b = 7.913(5) Å c = 19.351(1) Å V = 2077.8(3) Å^3
$Rb_3Bi_2Cl_9$ ($P12_1/a1$)	—	a = 13.3655(9) Å b = 7.9654(8) Å c = 15.423(1) Å V = 1641.8(2) Å^3

Table 2 Refined cell parameters for hybrid organic–inorganic compounds

	Reference	This work
$MA_3Bi_2I_9$ ($C12/c1$)	a = 8.4952(6) Å b = 14.7126(10) Å c = 21.6855(14) Å V = 2710.39 Å^3	a = 8.5340(5) Å b = 14.654(1) Å c = 21.653(1) Å V = 2707.9(3) Å^3
$FA_3Bi_2I_9$ ($C12/c1$)	—	a = 8.8389(8) Å b = 14.909(2) Å c = 21.851(3) Å V = 2879.5(6) Å^3
$MA_3Bi_2Br_9$ ($P\bar{3}m1$)	a = 8.188(2) Å b = 8.188(2) Å c = 9.927(3) Å V = 576.374 Å^3	a = 8.2086(2) Å b = 8.2086(2) Å c = 10.025(1) Å V = 585.03(6) Å^3
$FA_3Bi_2Br_9$ ($P\bar{3}m1$)	—	a = 8.4071(8) Å b = 8.4071(8) Å c = 10.183(2) Å V = 623.3(1) Å^3
$MA_3Bi_2Cl_9$ ($Pmcn$)	a = 7.713(8) Å b = 13.26(2) Å c = 20.43(3) Å V = 2089.47 Å^3	a = 7.7109(3) Å b = 13.2628(6) Å c = 20.4313(6) Å V = 2089.5(1) Å^3
$FA_3Bi_2Cl_9$ ($Pmcn$)	—	a = 8.045(1) Å b = 13.387(2) Å c = 21.062(3) Å V = 2268.3(6) Å^3

are more difficult to analyze as no reference patterns could be found for any $K_3Bi_2X_9$ compound. Nonetheless, when comparing the diffractograms after ball-milling with the reference patterns of the precursors (see Fig. S3, ESI†) it is clear that these have reacted to form a new phase, which it seems reasonable to attribute to $K_3Bi_2X_9$. This hypothesis is further supported by the optical absorption spectra (see Fig. 3).

Hybrid compounds with organic MA^+ and FA^+ cations were also formed by dry ball-milling of inorganic BiX_3 salts and organic AX (A = MA or FA). Again, when comparing X-ray diffractograms of the resulting MA-powders with reference bulk patterns from ICSD (see Fig. 2) we observe a very good match, highlighting the high phase purity of the mechanochemically-synthesized hybrid $MA_3Bi_2X_9$ compounds. To the best of our knowledge, only few reports on $FA_3Bi_2I_9$ exist,[10,17] while we were unable to find any reports on $FA_3Bi_2Br_9$ or $FA_3Bi_2Cl_9$. For the complete halide series, the diffractograms of the compounds obtained with FA closely match those of the corresponding MA analogues with a slight shift to lower angles, due to the higher ionic radius of FA compared to MA. Whole-pattern fits were conducted for all six hybrid compounds (see Fig. S4–S6, ESI†). Refined cell parameters confirm the cell expansion upon increase of the organic cation from MA to FA (see Table 2). Hence, again, we deduce the formation of highly phase-pure materials for all $FA_3Bi_2X_9$ compounds.

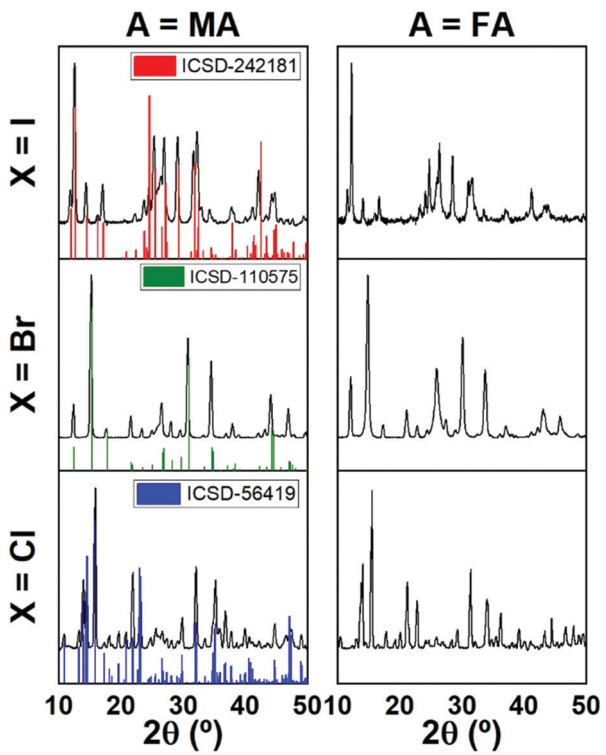

Fig. 2 XRD characterization of mechanochemically-synthesized hybrid $A_3Bi_2X_9$ (A = MA, FA; X = I, Br, Cl; black lines) and reference bulk patterns from the Inorganic Crystal Structure Database (ICSD) for A = MA (color columns). A more detailed comparison on diffractograms of same halide composition but different A-cation is presented in Fig. S4–S6 (ESI†). A broad feature around 2Θ = 26° is sometimes visible, due to the parasitic diffraction of the underlying adhesive tape used to fix the powder samples on the holder (see Fig. S1, ESI†).

The optical properties of the different inorganic and hybrid compounds (see Fig. 3) were analyzed by sandwiching the thin powders in between two quartz plates. The optical bandgaps of all materials, as derived from their absorption onsets (see Fig. 3) span from the near-UV (3.3 eV/380 nm for $K_3Bi_2Cl_9$) to the red part of the visible spectrum (1.9 eV/650 nm for $Cs_3Bi_2I_9$). Similar to what is observed in lead halide perovskites also for these "3-2-9" bismuth compounds the bandgap is strongly dependent on the X anion, with the smaller anion (Cl^-) giving the larger bandgaps and *vice versa*.[18] To a lesser extent, the same trend is visible with varying the ionic radius of the A-cation with X = Cl^- and X = Br^-. Indeed, for these halides we observe that the bandgap is systematically wider for A = K^+, followed by A = Rb^+ followed by the other cations. This trend, however, does not seem to apply for X = I^-. While the difference between the bandgaps of the iodide compounds is smaller (about 0.1 eV from 610 nm to 650 nm) as compared to the chloride series (about 0.3 eV difference corresponding to absorption onsets of

380 nm to 420 nm), it must be noted that, as opposed to 3D halide perovskites, these low-dimensional $A_3Bi_2X_9$ compounds crystallize in very different structures depending on their composition, as explained in the introduction (see Scheme 1). Hence, it is not surprising that the variations of optical properties with composition do not follow a homogenous trend for all cases. Moreover, we note the presence of a secondary absorption peak blue-shifted by *ca.* 50 nm in almost all compounds. Though the origin of this feature is unclear, it is consistent with previous reports on the same and related materials.[16,19] Despite the not yet encouraging results in photovoltaics,[3,20–22] these materials are promising candidates in electroluminescence applications.[8,23–28] A few recent reports have demonstrated high photoluminescence (PL) quantum yields from ligand-passivated colloidal nanoparticles of $Cs_3Bi_2Br_9$, $MA_3Bi_2Br_9$, and $MA_3Bi_2Cl_9$ in solution.[23,27–30] Others in contrast have not detected visible PL in similar colloidal quantum dots,[17] or achieved photoluminescence quantum yields lower than 1%.[31] Here, we show that mechanochemically-synthesized dry powders of $Cs_3Bi_2Br_9$ and $Cs_3Bi_2I_9$ show clearly visible PL at room temperature (see Fig. 3). This photoluminescence is slightly Stokes-shifted from the absorption edge, with maximums at 478 nm and 657 nm respectively for $X = Br^-$ and $X = I^-$. In both cases the PL spectrum is broad and asymmetric, consistent with previous reports.[23,27,28,31] As a result, the visible spectrum is almost fully-covered from 450 nm to 800 nm with these two compounds, which is of interest for the generation of white light. In order to demonstrate this, as a proof of concept, we fabricated a pellet by pressing a finely ground mixture of both powders with transparent PMMA beads. The corresponding PL spectrum (Fig. S7, ESI†) presents a broad emission with CIE coordinates (0.42; 0.45) corresponding to a warm white light with correlated color temperature of 3615 K.

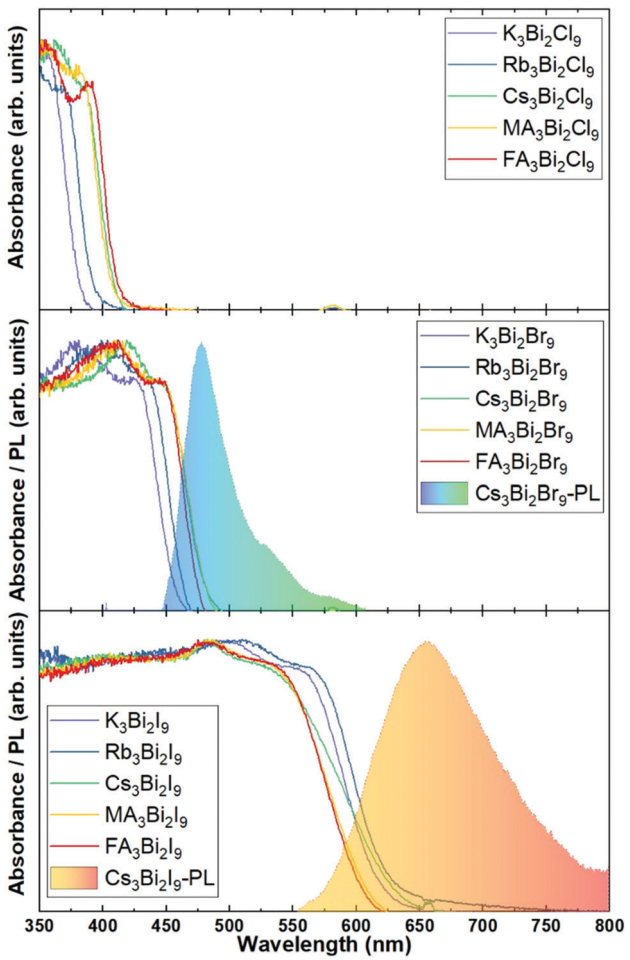

Fig. 3 Normalized absorbance spectra of all $A_3Bi_2X_9$ compounds (solid lines) and photoluminescence spectra of $Cs_3Bi_2Br_9$ and $Cs_3Bi_2I_9$ (dashed lines with filled area under curve).

Conclusions

In summary we have successfully synthesized fifteen different non-toxic bismuth halide ternary compounds by dry ball-milling of stoichiometric precursors. Structural characterization by X-ray diffraction revealed the excellent quality of the thus-formed materials, without noticeable unreacted precursors or byproducts. These materials have useful bandgaps for lighting applications as they cover most of the visible spectrum. Moreover, bulk dry $Cs_3Bi_2Br_9$ and $Cs_3Bi_2I_9$ exhibit photoluminescence at room temperature even without passivating agents. This holds promise to obtain high photoluminescence efficiency when passivating agents are added and paves the way to the widespread use of these non-toxic perovskite-related materials for lighting applications.

Conflicts of interest

There are no conflicts to declare.

Acknowledgements

The research leading to these results has received funding from the European Union Programme for Research and Innovation Horizon 2020 (2014-2020) under the Marie Skłodowska-Curie Grant Agreement PerovSAMs No. 747599, the Spanish Ministry of Economy and Competitiveness (MINECO) *via* the Unidad de Excelencia María de Maeztu MDM-2015-0538, MAT2017-88821-R and PCIN-2015-255, and the Generalitat Valenciana (Prometeo/2016/135 and GRISOLIAP/2017/089). H. J. B. acknowledges the support of ERA NET PCIN-2017-014. M. S. thanks the MINECO for his RyC contract.

References

1 J. L. Miller, *Phys. Today*, 2014, **67**, 13–15.
2 N. Leblanc, N. Mercier, L. Zorina, S. Simonov, P. Auban-Senzier and C. Pasquier, *J. Am. Chem. Soc.*, 2011, **133**, 14924–14927.
3 M. Lyu, J. H. Yun, M. Cai, Y. Jiao, P. V. Bernhardt, M. Zhang, Q. Wang, A. Du, H. Wang, G. Liu and L. Wang, *Nano Res.*, 2016, **9**, 692–702.
4 D. B. Mitzi, P. Brock, I. B. M. T. J. Watson, P. O. Box, Y. Heights, N. York, I. B. M. Almaden, H. Road, S. Jose and R. V. June, *Inorg. Chem.*, 2001, **40**, 2096–2104.

5 P. Szklarz, A. Pietraszko, R. Jakubas, G. Bator, P. Zieliński and M. Gałazka, *J. Phys.: Condens. Matter*, 2018, **20**, 255221.
6 N. C. Miller and M. Bernechea, *APL Mater.*, 2018, **6**, 084503.
7 T. Kawai, A. Ishii, T. Kitamura, S. Shimanuki, M. Iwata and Y. Ishibashi, *J. Phys. Soc. Jpn.*, 1996, **65**, 1464–1468.
8 K. M. McCall, C. C. Stoumpos, S. S. Kostina, M. G. Kanatzidis and B. W. Wessels, *Chem. Mater.*, 2017, **29**, 4129–4145.
9 M. Khazaee, K. Sardashti, J. P. Sun, H. Zhou, C. Clegg, I. G. Hill, J. L. Jones, D. C. Lupascu and D. B. Mitzi, *Chem. Mater.*, 2018, **30**, 3538–3544.
10 S. S. Shin, J. P. Correa Baena, R. C. Kurchin, A. Polizzotti, J. J. Yoo, S. Wieghold, M. G. Bawendi and T. Buonassisi, *Chem. Mater.*, 2018, **30**, 336–343.
11 T. Singh, A. Kulkarni, M. Ikegami and T. Miyasaka, *ACS Appl. Mater. Interfaces*, 2016, **8**, 14542–14547.
12 Y. El Ajjouri, F. Palazon, M. Sessolo and H. J. Bolink, *Chem. Mater.*, 2018, **30**, 7423–7427.
13 Y. El Ajjouri, V. S. Chirvony, M. Sessolo, F. Palazon and H. J. Bolink, *RSC Adv.*, 2018, **8**, 41548–41551.
14 A. D. Jodlowski, A. Yépez, R. Luque, L. Camacho and G. de Miguel, *Angew. Chem., Int. Ed.*, 2016, **55**, 14972–14977.
15 L. Protesescu, S. Yakunin, O. Nazarenko, D. N. Dirin and M. V. Kovalenko, *ACS Appl. Nano Mater.*, 2018, **1**, 1300–1308.
16 A. J. Lehner, D. H. Fabini, H. A. Evans, C. A. Hébert, S. R. Smock, J. Hu, H. Wang, J. W. Zwanziger, M. L. Chabinyc and R. Seshadri, *Chem. Mater.*, 2015, **27**, 7137–7148.
17 Q. A. Akkerman, L. Martínez-Sarti, L. Goldoni, M. Imran, D. Baranov, H. J. Bolink, F. Palazon and L. Manna, *Chem. Mater.*, 2018, **30**, 6915–6921.
18 Q. A. Akkerman, V. D'Innocenzo, S. Accornero, A. Scarpellini, A. Petrozza, M. Prato and L. Manna, *J. Am. Chem. Soc.*, 2015, **137**, 10276–10281.
19 S. Sun, S. Tominaka, J. H. Lee, F. Xie, P. D. Bristowe and A. K. Cheetham, *APL Mater.*, 2016, **4**, 031101.
20 B. W. Park, B. Philippe, X. Zhang, H. Rensmo, G. Boschloo and E. M. J. Johansson, *Adv. Mater.*, 2015, **27**, 6806–6813.
21 Z. Zhang, X. Li, X. Xia, Z. Wang, Z. Huang, B. Lei and Y. Gao, *J. Phys. Chem. Lett.*, 2017, **8**, 4300–4307.
22 H. Li, C. Wu, Y. Yan, B. Chi, J. Pu, J. Li and S. Priya, *ChemSusChem*, 2017, **10**, 3994–3998.
23 J. Pal, A. Bhunia, S. Chakraborty, S. Manna, S. Das, A. Dewan, S. Datta and A. Nag, *J. Phys. Chem. C*, 2018, **122**, 10643–10649.
24 K. K. Bass, L. Estergreen, C. N. Savory, J. Buckeridge, D. O. Scanlon, P. I. Djurovich, S. E. Bradforth, M. E. Thompson and B. C. Melot, *Inorg. Chem.*, 2017, **56**, 42–45.
25 C. W. M. Timmermans and G. Blasse, *Phys. Status Solidi*, 1981, **647**, 647–655.
26 G. M. Paternò, N. Mishra, A. J. Barker, Z. Dang, G. Lanzani, L. Manna and A. Petrozza, *Adv. Funct. Mater.*, 2018, **1805299**, 1–6.
27 M. Leng, Z. Chen, Y. Yang, Z. Li, K. Zeng, K. Li, G. Niu, Y. He, Q. Zhou and J. Tang, *Angew. Chem., Int. Ed.*, 2016, **55**, 15012–15016.
28 M. Leng, Y. Yang, Z. Chen, W. Gao, J. Zhang, G. Niu, D. Li, H. Song, J. Zhang, S. Jin and J. Tang, *Nano Lett.*, 2018, **18**, 6076–6083.
29 A. Sarkar, P. Acharyya, R. Sasmal, P. Pal, S. S. Agasti and K. Biswas, *Inorg. Chem.*, 2018, **57**, 15558–15565.
30 L. Lian, G. Zhai, F. Cheng, Y. Xia, M. Zheng, J. Ke, M. Gao, H. Liu, D. Zhang, L. Li, J. Gao, J. Tang and J. Zhang, *CrystEngComm*, 2018, **20**, 7473–7478.
31 B. Yang, J. Chen, F. Hong, X. Mao, K. Zheng, S. Yang, Y. Li, T. Pullerits, W. Deng and K. Han, *Angew. Chem., Int. Ed.*, 2017, **56**, 12471–12475.

